Supplemental Discussion for Multijunction Solar Cell Efficiencies: Effect of Spectral Window, Optical Environment and Radiative Coupling

Carissa N. Eisler,[1] Ze'ev R. Abrams,[2] Matthew T. Sheldon,[1] Xiang Zhang,[2] Harry A. Atwater[1]

[1]Thomas J. Watson Laboratories of Applied Physics, California Institute of Technology, Pasadena, CA 91125, USA

[2]Materials Science Division Lawrence Berkeley National Laboratory, 1 Cyclotron Road, Berkeley, CA 94720, USA

Further Discussion and Derivation of Two Subcell Model

Here we derive the expressions used in the manuscript. We approximate the sun as a blackbody radiator with a temperature of T_S (6000° K) and with a solid angle θ_s (0.267°).[1] The data in the Letter are derived instead for subcells under 1 sun AM1.5D G173-03 illumination. The expression for subcell power can easily be derived for the AM1.5D spectrum by substituting the numerical integral of AM1.5D photon flux for the 6000°K blackbody radiation. However, a simple analytic solution for the open-circuit voltage for the AM1.5D cannot be determined because the integral can only be solved numerically. Therefore we derive the equations for the two subcell model under blackbody illumination so the reader may observe the direct impact of radiative coupling and spectral window on subcell voltage.

Each subcell is maintained at an ambient temperature T_o (300° K) and is reradiating photons with energies above its bandgap within the half angle of emission, θ_E.[1,2] We assume no concentration and a perfect back reflector such that $\theta_E = \pi/2$.[3] We also assume that there are no reflection losses and that any subcell perfectly absorbs photons with energies equal to or above its bandgap.

We first analyze subcell #1 because it is not affected by subcell #2. We are only observing structures with few enough subcells such that downshifting is the only relevant form of radiative coupling. Subcell #1 acts as a single junction cell and will have an identical analysis to the Shockley-Queissar derivation.[1] The power extracted from subcell #1 is:

$$P_1 = V_1 J_1 = \frac{2\pi q V_1}{h^3 c^2}\left(\sin^2(\theta_s)\int_{E_g+\Delta}^{\infty}\frac{E^2 dE}{\exp\left(\frac{E}{kT_s}\right)-1} - \int_{E_g+\Delta}^{\infty}\frac{E^2 dE}{\exp\left(\frac{E-qV_1}{kT_o}\right)-1}\right) \qquad (1s)$$

where V is the operating voltage of a subcell, J is the current produced in a subcell, q is the charge of an electron, h is Planck's constant, and c is the speed of light, and k is Boltzmann's constant. Because each subcell has a perfect back reflector on the rear interface, the radiative prefactor ($\frac{2\pi q}{h^3c^2}(n_{top}{}^2 + n_{bot}{}^2)$) reduces to show that radiative emission only occurs out the front interface ($\frac{2\pi q}{h^3c^2}$).

Now we calculate the power extracted from subcell #2. Unlike the analysis for subcell #1, there will be three current terms in the expression for subcell #2 because there are three photon fluxes. The first current term comes from the input spectrum, which only includes photons within the spectral window, *Δ*. The current term is from reradiating photons from subcell #1, and this is calculated using the dark current expression from equation (1s) and multiplying by B to account for the actual fraction of photons distributed from subcell #1 to subcell #2. Finally, there is a dark current term associated with the photons reradiated from subcell #2.

$$P_2 = V_2 J_2 = V_2 \frac{2\pi q}{h^3c^2}\left[\sin^2(\theta_s)\int_{E_g}^{E_g+\Delta}\frac{E^2 dE}{\exp\left(\frac{E}{kT_s}\right)-1} + B\int_{E_g+\Delta}^{\infty}\frac{E^2 dE}{\exp\left(\frac{E-qV_1}{kT_o}\right)-1}\right.$$
$$\left. - \frac{1}{ERE_2}\int_{E_g}^{\infty}\frac{E^2 dE}{\exp\left(\frac{E-qV_2}{kT_o}\right)-1}\right] \qquad (2s)$$

The operating voltage is calculated when the power in Equations (1s) and (2s) is maximized.

We also examine the open-circuit voltage condition, which occurs when there is no current produced in the cell. Again, we begin by deriving the expression for subcell #1 and show the condition for open-circuit voltage below:

$$\sin^2(\theta_s)\int_{E_g+\Delta}^{\infty}\frac{E^2 dE}{\exp\left(\frac{E}{kT_s}\right)-1} = \int_{E_g+\Delta}^{\infty}\frac{E^2 dE}{\exp\left(\frac{E-qV_{oc,1}}{kT_o}\right)-1} \qquad (3s)$$

The photon flux of input photons is exactly balanced by the photon flux of reradiating photons. We perform this same analysis for subcell #2:

$$\sin^2(\theta_s) \int_{E_g}^{E_g+\Delta} \frac{E^2 dE}{\exp\left(\frac{E}{kT_s}\right) - 1} + B \int_{E_g+\Delta}^{\infty} \frac{E^2 dE}{\exp\left(\frac{E - qV_{oc,1}}{kT_o}\right) - 1}$$
$$= \frac{1}{ERE_2} \int_{E_g+\Delta}^{\infty} \frac{E^2 dE}{\exp\left(\frac{E - qV_{oc,2}}{kT_o}\right) - 1} \quad (4s)$$

We can describe this added flux of reradiating photons from subcell #1 as the right side of equation (3s) multiplied by the geometric factor *B*. We then obtain

$$\sin^2(\theta_s) \left(\int_{E_g}^{E_g+\Delta} \frac{E^2 dE}{\exp\left(\frac{E}{kT_s}\right) - 1} + B \int_{E_g+\Delta}^{\infty} \frac{E^2 dE}{\exp\left(\frac{E}{kT_s}\right) - 1} \right)$$
$$= \frac{1}{ERE_2} \int_{E_g+\Delta}^{\infty} \frac{E^2 dE}{\exp\left(\frac{E - qV_{oc,2}}{kT_o}\right) - 1} \quad (5s)$$

We then rearrange the integrals in the right hand side of equation (5s) for the following revised expression.

$$\sin^2(\theta_s) \left(\int_{E_g}^{\infty} \frac{E^2 dE}{\exp\left(\frac{E}{kT_s}\right) - 1} + (B - 1) \int_{E_g+\Delta}^{\infty} \frac{E^2 dE}{\exp\left(\frac{E}{kT_s}\right) - 1} \right)$$
$$= \frac{1}{ERE_2} \int_{E_g+\Delta}^{\infty} \frac{E^2 dE}{\exp\left(\frac{E - qV_{oc,2}}{kT_o}\right) - 1} \quad (6s)$$

Equation (6s) now looks very similar to the open-circuit voltage condition for a single junction solar cell but has an additional term to account for the spectral width and radiative coupling. Using a standard approximation for these integrals that is valid for low concentration and for $E_g \gg kT_s$ and $E_g - qV_{oc} \gg kT_o$, an approximated expression for $V_{oc,2}$ is derived.[4]

$$qV_{oc,2} \cong E_g \left(1 - \frac{T_o}{T_s}\right) + kT_o \ln(\sin^2(\theta_s)) + kT_o \ln\left(\frac{T_s}{T_o}\right)$$
$$+ kT \ln(\alpha_1) + kT_o \ln(ERE_2) + kT_o \ln\left[1 + (B - 1)\left(\frac{\alpha_\Delta}{\alpha_1}\right) \exp\left(-\frac{\Delta}{kT_s}\right)\right] \quad (7s)$$

where the terms α_1 and α_Δ are $1+2kT_S/E_g+2(kT_S/E_g)^2$ and $\alpha_1+2\Delta/E_g+(\Delta/E_g)^2+2kT_S\Delta/E_g$, respectively, and are correction terms for approximating the integrals.[5,6] In Equation (7s), we identify the first term as the Carnot efficiency and the second term to be an entropic loss due to lack of angle restriction, reducing the available free energy in the system.[5,7] The third and fourth terms as corrections to account for the broadband range of the spectra. We also recognize these first four terms together comprise the open-circuit voltage of a single junction cell. We combine these terms and represent them as $V_{oc,2}{}^{SQ}$ and simplify to obtain our final expression:

$$qV_{oc,2} \cong qV_{oc,2}^{SQ} + kT_o \ln\left[1 + (B-1)\left(\frac{\alpha_\Delta}{\alpha_1}\right)\exp\left(-\frac{\Delta}{kT_s}\right)\right] \tag{8s}$$

A decrease in spectral window (Δ) will decrease the open-circuit voltage. However, this loss is minimized for higher values of B and is eliminated when B=1 because all photons are downshifted from subcell #1 to subcell #2.

Additional Experimental Methods

Alta Devices provided thin-film, epitaxially lifted-off GaAs solar cells for the experimental portion of this study. The light *I-V* response of the cell was measured under 100 mW cm^{-2} of simulated AM1.5G illumination using a Keithley 238 high current source measure unit. A longpass filter was placed above the cell to block higher energy photons in the input spectrum, varying the spectral window. The filters used blocked wavelengths shorter than 430 nm (Chroma ET430lp), 550 nm (Newport 10LWF-550-B), 580 nm (Chroma HQ580lp), 630 nm (Chroma HQ630lp), 650 nm (Thorlabs FEL650), 700 nm (Thorlabs FEL700), and 850 nm (Thorlabs 850nm).

To analyze the data properly, we modify Equation (2s) to better describe the experimental conditions and nonidealities of the cell. We first reduce Equation (2s) for the B=0 case.

$$P_2 = V_2 J_2 = V_2 \frac{2\pi q}{h^3 c^2}\left[\sin^2(\theta_s)\int_{E_g}^{E_g+\Delta} \frac{E^2 dE}{\exp\left(\frac{E}{kT_s}\right)-1} - \frac{1}{ERE_2}\int_{E_g}^{\infty} \frac{E^2 dE}{\exp\left(\frac{E-qV_2}{kT_o}\right)-1}\right] \tag{9s}$$

We recognize that our input spectra is not a blackbody radiator, so we adjust the input current to account for the 1 sun AM1.5G spectrum by integrating over the photon flux $N_{AM1.5G}$. Additionally, we include the absorbance of the semiconductor slab (a(E)) and a reflection loss due to the lack of an antireflection coating (R). We also add the external radiative efficiency (*ERE*) to account for nonradiative recombination and parasitic losses in the back reflector. The *ERE* is a good measure of cell quality because it is related to the internal radiative efficiency, or how likely a cell is to recombine radiatively instead of nonradiatively.[8,9]

$$P_2 = V_2 J_2 = V_2 \frac{2\pi q}{h^3 c^2} \left[(1-R) \int_{E_g}^{E_g+\Delta} a(E) N_{AM1.5G}(E) dE - \frac{1}{ERE_2} \int_{E_g}^{\infty} \frac{E^2 dE}{\exp\left(\frac{E - qV_2}{kT_o}\right) - 1} \right] \quad (10s)$$

Finally, we adjust this expression to include series (R_s) and shunt resistances (R_{sh}) following expressions from literature.[10] This yields the following recursive function:

$$P_2 = V_2 J_2 = V_2 \left[\left((1-R) \int_{E_g}^{E_g+\Delta} a(E) N_{AM1.5G}(E) dE - \frac{1}{ERE_2} \frac{2\pi q}{h^3 c^2} \int_{E_g}^{\infty} \frac{E^2 dE}{\exp\left(\frac{E - q(V_2 + I_2 R_s)}{kT_o}\right) - 1} \right) - \frac{V_2 + I_2 R_s}{R_{sh}} \right] \quad (11s)$$

We calculated reflection losses by comparing the measured J_{sc} to the maximum theoretical J_{sc} for a GaAs cell under AM1.5G illumination. This was equal to 35%, which corresponds to the reflection losses between air and a high index semiconductor. The external radiative efficiency was calculated in a similar way, comparing the actual V_{oc} to the maximum V_{oc} attainable with the realistic J_{sc}. Accounting for the nonradiative losses of the experimental cells corresponds to an *ERE* of 3.9% which is comparable to other GaAs solar cells of similar growth quality and back reflector type.[4,5] Finally, we calculated series and shunt resistances of 2.5 and 2779 Ω/cm^2, respectively, by inspecting the slope of the I-V curve near V_{oc} and J_{sc}.[10] Incorporating these parameters provided an excellent fit to our data.

Additional Equations for Full Multijunction Ensemble Efficiency Calculations

The efficiencies for Fig. 3 were determined by summing the power produced in each subcell and dividing by the total power in the solar spectrum under 1 sun AM1.5D G173-03 conditions. These also assume that radiative emission is the only loss mechanism, yielding the maximum efficiency possible for the geometry. Also, all cases with radiative coupling assume that absorption of radiatively emitted photons only occurs when the absorbing subcell has a smaller bandgap than the emitting subcell. This is valid in the regime we study (number of subcells $\leq$ 20). The power produced in a given subcell for the *B* cases (i.e. architectures that allow radiative coupling between subcells and back reflectors on all subcells) presented in the paper ($P_{n,B}$) is a more general case of Equation (2s), as shown below:

$$P_{n,B} = V_n J_n = V_n \left[\int_{E_{g,n}}^{E_{g,n-1}} N_{AM1.5D}(E) dE + \frac{2\pi q}{h^3 c^2} \left(B \int_{E_{g,n-1}}^{\infty} \frac{E^2 dE}{\exp\left(\frac{E - qV_{n-1}}{kT_o}\right) - 1} - \int_{E_{g,n}}^{\infty} \frac{E^2 dE}{\exp\left(\frac{E - qV_n}{kT_o}\right) - 1} \right) \right] \quad (12s)$$

where *n* refers to the current subcell and *n-1* is the subcell with the next highest bandgap. Because we only discuss downshifting structures, we first calculate the power produced in the subcell with the highest bandgap and then continue in order of decreasing bandgap such that the subcell with the lowest bandgap is calculated last. We again note that each subcell has a perfect back reflector on the rear interface so the radiative prefactor ($\frac{2\pi q}{h^3 c^2}({n_{top}}^2 + {n_{bot}}^2)$) reduces to show that radiative emission only occurs out the front interface ($\frac{2\pi q}{h^3 c^2}$).

The power produced in a given subcell for the traditional and air gap tandem stack cases can be described by a similar equation, which is given below. Again there are three terms that describe the current generated from the spectral window of the sun, the current generated from radiative coupling with subcell *n-1*, and the dark current due to radiative emission.

$$P_{n,TS} = \begin{cases} V_n \left[\int_{E_{g,n}}^{E_{g,n-1}} N_{AM1.5D}(E) dE + \frac{2\pi q}{h^3 c^2}({n_{top}}^2 + {n_{bot}}^2) \left(\left(\frac{{n_{bot}}^2}{{n_{top}}^2 + {n_{bot}}^2} \right) \int_{E_{g,n-1}}^{\infty} \frac{E^2 dE}{\exp\left(\frac{E - qV_{n-1}}{kT_o}\right) - 1} - \int_{E_{g,n}}^{\infty} \frac{E^2 dE}{\exp\left(\frac{E - qV_n}{kT_o}\right) - 1} \right) \right], n < N \\ V_n \left[\int_{E_{g,N}}^{E_{g,N-1}} N_{AM1.5D}(E) dE + \frac{2\pi q}{h^3 c^2} \left(({n_{top}}^2 + {n_{bot}}^2) \left(\frac{{n_{bot}}^2}{{n_{top}}^2 + {n_{bot}}^2} \right) \int_{E_{g,N-1}}^{\infty} \frac{E^2 dE}{\exp\left(\frac{E - qV_{N-1}}{kT_o}\right) - 1} - ({n_{top}}^2) \int_{E_{g,N}}^{\infty} \frac{E^2 dE}{\exp\left(\frac{E - qV_N}{kT_o}\right) - 1} \right) \right], n = N \end{cases} \quad (13s)$$

We keep the general form of the radiative prefactor ($\frac{2\pi q}{h^3 c^2}({n_{top}}^2 + {n_{bot}}^2)$) to reflect the different optical environment of this geometry (i.e. include the index of refraction of the substrates or air interface since the subcells are no longer on perfect back reflectors). Only the bottom subcell (n=N) has a back reflector in these tandem stack cases so the radiative prefactor reduces to $\frac{2\pi q}{h^3 c^2}{n_{top}}^2$. Additionally, the degree of radiative coupling is now determined by the refractive index contrast between the top and bottom interfaces (${n_{bot}}^2/{n_{top}}^2 + {n_{bot}}^2$). These expressions are derived in other studies.[2,3]

The only difference between these two cases is the optical environment. The traditional tandem stack has n_{top} = 1 and n_{bot} = 3.6 (the refractive index of a III-V semiconductor) while the air gap tandem stack has n_{top} = 1 and n_{bot} = 1. Although all subcells *n*>1 in the traditional tandem stack share a perfect top interface with another subcell, we operate in the regime ($N \leq 20$) where the radiative emission from subcell *n+1* does not overlap with the bandgap, and absorption profile, of subcell *n*. Therefore the relevant top interface for every subcell is air ($n_{top} = 1$) in this regime. Additionally, this will cause the traditional tandem stack will have a higher degree of radiative coupling but a higher dark current because of the index matching between subcells and high index contrast of the top air interface. In the regime of many subcells ($N >> 20$), the radiative emission from subcell *n+1* would have to be included and *B* would have to be adjusted accordingly.

The power produced in a selective reflector structure is given below by Equation 14s. This structure has no radiative coupling and therefore the current is comprised only of the generated current from the solar spectral window and the radiative dark current. The radiative prefactor on the radiative emission also reduces to $\frac{2\pi q}{h^3 c^2}$ because the subcells can only radiate out the front face due to the selective reflector. Unlike the previous structures, the radiative emission is restricted by energy owing to the selective reflectors[2] but this effect is negligible in the regime we study ($N \leq 20$ subcells).

$$P_{n,SR} = V_n J_n = V_n \left[\int_{E_{g,n}}^{E_{g,n-1}} N_{AM1.5D}(E) dE - \frac{2\pi q}{h^3 c^2} \int_{E_{g,n}}^{E_{g,n-1}} \frac{E^2 dE}{\exp\left(\frac{E - qV_n}{kT_o}\right) - 1} \right] \qquad (14s)$$

The power produced by the PSR is given below. It is very similar to the radiative coupling cases discussed earlier, but has two additional terms: (1) C_{geom}, which represents the reduced concentration from placing cells at an angle relative to the input aperture, (2) RB_n, which represents the fraction of photons that are reflected back into the same subcell. Similar to the *B* cases, the radiative prefactor is reduced to $\frac{2\pi q}{h^3 c^2}$ because the subcells are spatially separated and have their own back reflector. The values for C_{geom}, B_n, and RB_n are derived in the next section.

$$\begin{aligned} P_{n,PSR} = V_n J_n = V_n \Bigg[& C_{geom} \int_{E_{g,n}}^{E_{g,n-1}} N_{AM1.5D}(E) dE \\ & + \frac{2\pi q}{h^3 c^2} \left(B_n \int_{E_{g,n-1}}^{\infty} \frac{E^2 dE}{\exp\left(\frac{E - qV_{n-1}}{kT_o}\right) - 1} - (1 - RB_n) \int_{E_{g,n}}^{\infty} \frac{E^2 dE}{\exp\left(\frac{E - qV_n}{kT_o}\right) - 1} \right) \Bigg] \end{aligned} \qquad (15s)$$

Calculating Concentration, Radiative Coupling, and Light Trapping for the PSR

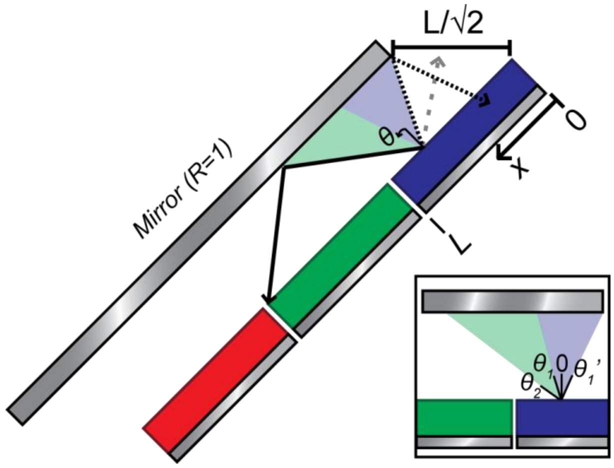

Figure 1s. Schematic of the 45° polyhedral specular reflector (PSR) design studied in the Letter. The blue cone represents the angular range of photons that are reflected back into the same subcell at that example point. The green cone represents the range of angles of photons that are emitted into the next subcell. The inset shows the relevant angles for radiative emission discussed.

A schematic of the polyhedral specular reflector is shown in Figure 1s. The first subcell always covers the full aperture opening to have photons encounter each subcell in order from highest to lowest bandgap. Otherwise the spectrum will not be split properly. For this Letter, the subcells are arranged at a 45° angle. For a subcell length of L, the aperture of the multijunction cell is $L/\sqrt{2}$. This geometry will determine both the concentration on each subcell and the final destination of the radiatively emitted photons. For a 45° PSR, the concentration factor is $1/\sqrt{2}$, the ratio of the subcell to the input aperture.

To determine the fraction of photons reflected back into the same subcell (RB_n) and the fraction of photons downshifted to the next bandgap (B_n), the destination of each photon as a function of angle is determined as a function of position and this is averaged over the length of the subcell (L). For the example photons shown in Figure 1s, emitted photons occupying the angles of the blue cone (θ_1 to θ_1') will be reflected back into the same subcell and represent RB_n. The emitted photons occupying the green cone (θ_1 to θ_2) will be reflected to the next subcell and represent B_n. These cones will change as a function of position, so we determine the average angle occupancy as a function of x. Then we integrate that expression over the length of the cell, normalizing by L, as outlined below for calculating the fraction of photons reflected back into the same subcell.

$$\text{Fraction of photons reflected back onto same subcell as a function of } x = \frac{\int_{\theta_1'(x)}^{\theta_1(x)} \cos(\alpha)\, d\alpha}{\int_0^{\pi/2} \cos(\alpha)\, d\alpha}$$

$$\text{Fraction of photons reflected back onto same subcell averaged over entire subcell} = \frac{\int_0^L \sin(\theta_1(x)) - \sin(\theta_1'(x))\, dx}{\int_0^L dx}$$

This same process is repeated for determining the fraction of photons reflected to the next subcell. This yields a B_n of 0.204 for all subcells and an RB_n of 0.414 for all subcells except the first in the stack (n>1). The fraction of photons reflected back onto the same subcell is different for the first subcell (blue in Figure 1s) because the mirror does not completely cover the first subcell, which is a consequence of having the aperture wide enough to project the illuminated area across the whole length of the first subcell. Thus the RB_1 of the first subcell is 0.207.

It should also be noted that the geometry of the PSR (angle and aperture size) can be adjusted to yield different values for C_{geom}, *RB*, and *B*. For example, the aperture size can be reduced which will bring the mirror closer to the subcells, increasing the number of angles that fall within the cone of light that is reflected back into the same subcell (increasing *RB*). However, this also reduces the concentration of incident light on each subcell and reduces the number of downshifted photons (*B*). Additionally, the angle of the PSR can be reduced. This will decrease the concentration loss (aperture to cell length ratio is smaller) but will reduce *RB* and *B*.

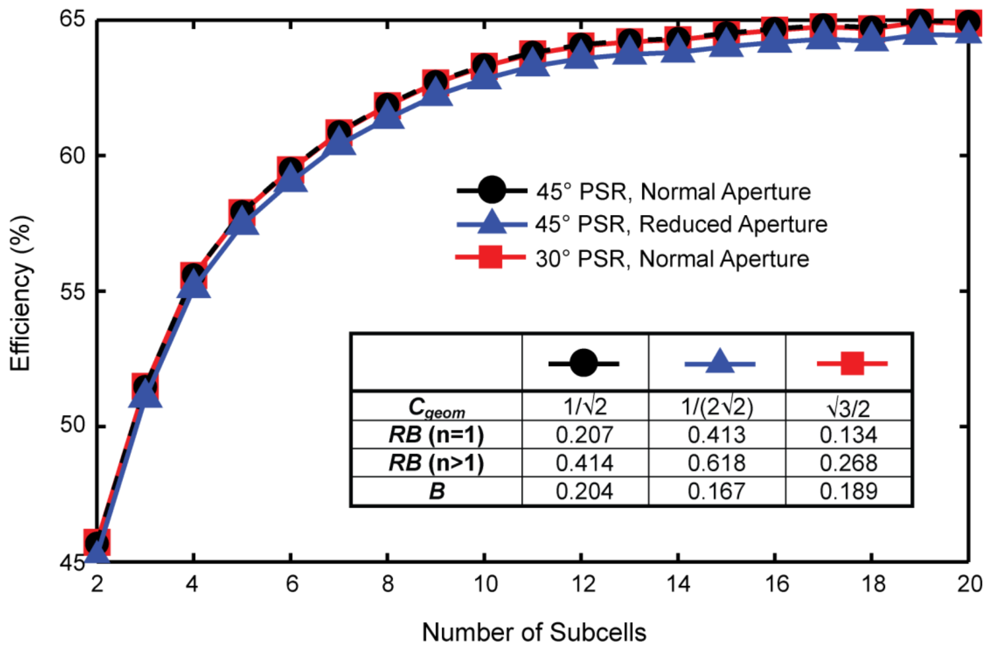

Figure 2s. Efficiency versus number of subcells for different PSR geometries: the 45° PSR presented in the paper (black circle), a 45° PSR with a reduced input aperture size (blue triangle), and a 30° PSR (red square). The inset shows the relevant parameters (C_{geom}, *RB*, and *B*) for each geometry.

Figure 2s shows the efficiency as a function of number of subcells for the three PSR geometries and the inset displays the values for C_{geom}, *RB*, and *B*. Although the reduced aperture 45° PSR has a much larger *RB* because of the new mirror spacing, the reduced concentration reduces the overall efficiency beyond any additional light trapping benefit. Additionally, changing the angle of the PSR to 30° slightly increases the efficiency for a 2 and 3 subcell structure but slightly decreases the efficiency beyond the 45° PSR for cells with 4 or more subcells. The 30° PSR has smaller *RB* and *B* values than the original 45° PSR but it has a significantly larger concentration factor. Therefore for a small number of subcells (<4), the concentration factor is more important and the 30° PSR is most efficient. For a larger number of subcells (≥4), the increased light trapping and radiative coupling of the 45° PSR makes it more efficient than the 30° PSR. Therefore the geometry of the PSR can be optimized depending on the number of subcells and performance of the optical components.

Bandgaps Used in Figure 3

The following tables depict the bandgaps used in Figure 3 of the paper. They were optimized from the work from E. Warmann, et. al.[11]

No. Subcells	2	3	4	5	6	7	8	9	10	11
Bandgaps (eV)	0.94	0.94	0.7	0.69	0.69	0.69	0.51	0.51	0.51	0.51
	1.64	1.39	1.12	0.99	0.95	0.94	0.7	0.7	0.7	0.7
		2	1.55	1.38	1.33	1.15	0.94	0.94	0.94	0.94
			2.16	1.81	1.61	1.39	1.14	1.14	1.13	1.13
				2.35	2.01	1.71	1.39	1.39	1.34	1.34
					2.5	2.07	1.71	1.64	1.53	1.53
						2.5	2.07	1.91	1.75	1.73
							2.52	2.23	2	1.94
								2.66	2.3	2.19
									2.66	2.5
										2.89

No. Subcells	12	13	14	15	16	17	18	19	20
Bandgaps (eV)	0.51	0.51	0.5	0.51	0.51	0.5	0.5	0.5	0.5
	0.7	0.7	0.69	0.7	0.7	0.55	0.56	0.54	0.57
	0.93	0.93	0.77	0.93	0.92	0.7	0.7	0.69	0.7
	1.12	1.12	0.94	1.11	1	0.77	0.78	0.75	0.78
	1.33	1.33	1.13	1.22	1.12	0.93	0.93	0.92	0.93
	1.47	1.47	1.33	1.37	1.22	1.11	1.01	0.99	0.99
	1.64	1.64	1.47	1.51	1.37	1.2	1.12	1.13	1.12
	1.81	1.81	1.64	1.64	1.51	1.34	1.22	1.22	1.2
	2	2	1.81	1.81	1.64	1.44	1.37	1.35	1.33
	2.23	2.21	1.98	1.98	1.81	1.55	1.51	1.45	1.41
	2.51	2.42	2.16	2.16	1.98	1.71	1.64	1.55	1.53
	2.89	2.66	2.38	2.38	2.16	1.86	1.75	1.67	1.65
		2.98	2.61	2.61	2.38	2	1.89	1.82	1.77
			2.93	2.89	2.61	2.18	2.02	1.99	1.9
				3.25	2.89	2.38	2.21	2.16	2.06
					3.25	2.66	2.4	2.38	2.21
						3	2.64	2.61	2.37
							2.95	2.87	2.56
								3.22	2.83
									3.16

References

1 W. Shockley & H. J. Queisser, *J. Appl. Phys.* **32**, 510 (1961).

2 A. Martí & G. L. Araújo, *Sol. Energ. Mat. Sol. C.* **43**, 203-222 (1996).

3 M. A. Green, *Prog. Photovoltaics* **20**, 127-134 (2012).

4 W. Ruppel & P. Wurfel, *IEEE T. Electron Dev.* **27**, 877-882 (1980).

5 T. Markvart, *Appl. Phys. Lett.* **91**, 064102 (2007).

6 A. Niv, Z. R. Abrams, M. Gharghi, C. Gladden, and X. Zhang, Applied Physics Letters **100**, 083901 (2012).

7 T. Markvart, *Journal of Optics a-Pure and Applied Optics* **10**, (2008).

8 O. D. Miller, E. Yablonovitch, & S. R. Kurtz, *IEEE Journal of Photovoltaics* **2**, 303 (2012).

9 M. A. Green, *Prog. Photovoltaics* **20**, 472-476, (2012).

10 J. L. Gray, *Handbook of Photovoltaic Science and Engineering*. (eds A. Luque & S. Hegedus) 102-104 (John Wiley & Sons, 2003).

11 E. C. Warmann, C. N. Eisler, E. D. Kosten, M. Escarra, and H. A. Atwater, in *Photovoltaic Specialists Conference (PVSC), 2013 39th IEEE*, 2013).